Korean J. Chem. Eng., 38(3), 540-551 (2021)
DOI: 10.1007/s11814-020-0713-0

pISSN: 0256-1115
eISSN: 1975-7220

Computational fluid dynamics simulation of methanol to olefins in stage circulating fluidized bed riser: Effect of reactor stage parameters on product yields

Chaiwat Soanuch*, Krittin Korkerd*, Jakkrapong Phupanit, Ratchanon Piemjaiswang***, Pornpote Piumsomboon*,****, and Benjapon Chalermsinsuwan*,****,*****,†**

*Department of Chemical Technology, Faculty of Science, Chulalongkorn University, 254 Phyathai Road, Wangmai, Pathumwan, Bangkok 10330, Thailand
**Program in Petrochemistry and Polymer Science, Faculty of Science, Chulalongkorn University, 254 Phayathai Road, Wangmai, Pathumwan, Bangkok 10330, Thailand
***Environmental Research Institute, Chulalongkorn University, 254 Phyathai Road, Wangmai, Pathumwan, Bangkok 10330, Thailand
****Center of Excellence on Petrochemical and Materials Technology, Chulalongkorn University, 254 Phayathai Road, Wangmai, Pathumwan, Bangkok 10330, Thailand
*****Advanced Computational Fluid Dynamics Research Unit, Chulalongkorn University, 254 Phyathai Road, Wangmai, Pathumwan, Bangkok 10330, Thailand
(*Received 12 July 2020 • Revised 3 November 2020 • Accepted 16 November 2020*)

Abstract−The risers of a conventional fluidized bed reactor and a stage fluidized bed reactor for the convention of methanol to olefins (MTO) were simulated using computational fluid dynamics. The reaction rates of the MTO reaction were validated to successfully match with the literature experiment. Then, the reactor stage parameters were examined by using the 2^k design of the experiment method, including the number of reactor stages, the thickness of the reactor stage, and the wall temperature of the reactor stage. The stage circulating fluidized bed riser decreased the yield of ethene but increased the yield of propene and light olefins. From the obtained solid volume fraction profile, the stage circulating fluidized bed riser could reduce the back-mixing and increase the system turbulence, which promotes the light olefins of the MTO reaction yield. The wall temperature of the reactor stage did not significantly affect the chemical reaction in the circulating fluidized bed riser.

Keywords: Circulating Fluidized Bed Riser, Computational Fluid Dynamics, Methanol to Olefins, Stage, Simulation

INTRODUCTION

The circulating fluidized bed reactor is widely used for a gas-solid particle multi-phase flow system. It consists of a riser, downer, cyclone, and return system [1]. The distinct advantage of this reactor is its excellent heat transfer, which then can remove or add the heat from exothermic or endothermic chemical reactions. In addition, the catalyst solid particle for a heterogeneous chemical reaction can be continuously reacted and regenerated in the circulating fluidized bed riser and downer, respectively. Various heterogeneous catalytic chemical reactions can occur in the circulating fluidized bed reactor, such as the synthesis of synthetic gas [2], steam reforming of natural gas [3,4], gasification of coal [5], or polyolefin production [6]. One of the promising heterogeneous catalytic chemical reaction applications in the circulating fluidized bed reactor is the methanol to olefins reaction (MTO). The MTO reaction is an alternative chemical reaction process to produce essential chemicals in the petrochemical industry, such as ethene and propene, from methanol [7,8]. Ethene can be a raw material for housewares and food packaging, while propene can be a raw material for pipes and the construction of automotive components [9,10]. Therefore, the demand for ethene and propene is growing [11,12]. The methanol conversion requires a specific solid particle catalyst to produce olefins [13,14]. Conventionally, there are many processes to produce these olefins, including thermal cracking [15] and fluid catalytic cracking [16,17] using naphtha or other petroleum as feedstock. However, these processes are energy-intensive and produce a low olefin yield. Therefore, the MTO reaction is proposed as new technology to overcome the problems of the conventional processes.

The hydrodynamic behavior and chemical reaction behavior have already been studied in a fixed bed reactor [18-20], fluidized bed reactor [21,22], and circulating fluidized bed reactor [23,24] using both experiment and computational fluid dynamics (CFD) approaches. It was observed that non-homogeneous gas-solid particle behavior led to the decrease of the chemical reaction inside these reactors [25-27]. Recently, the modification of circulating fluidized bed reactors, especially in circulating fluidized bed risers, was recommended to make the reactor system more homogeneous, such as the addition of the reactor stage and internal [1,28]. The flow dynamic behavior in the reactor systems changed when the reactor systems were disturbed. The pressure drop with a three-stage fluidized bed reactor was lower than the conventional fluid-

†To whom correspondence should be addressed.
E-mail: benjapon.c@chula.ac.th
Copyright by The Korean Institute of Chemical Engineers.

ized bed reactor [29]. In the literature, the gas turbulence increased and the solid particle back-mixing decreased when louver baffles were installed in the circulating fluidized bed riser [28,30]. Therefore, installing the baffles significantly led to preferable system hydrodynamics, but this addition may agilely erode in an actual fluidized bed system [31]. The stage of the fluidized bed reactor increased the residence time of the catalyst solid particles. It then reduced solid particle back-mixing and increased the heat transfer, which was more desirable than the conventional fluidized bed reactor, the fixed bed reactor, and the circulating fluidized bed reactor [32,33]. Also, the conversion and yield of the MTO reaction in the fluidized bed reactor were affected by the reactor operating parameters, including the gas superficial velocity, the amount of catalyst solid particles, the initial coke content of the catalyst solid particle, and the reactor temperature [34,35]. From the advantage of stage circulating fluidized bed risers, the effect of reactor stage parameters on each product yield was thus of interest in applying with the MTO reaction.

This study aimed to develop the CFD model and to study the system hydrodynamics and the MTO reaction in a two-dimensional stage circulating fluidized bed riser (e.g., 2 and 4 stages). When the system was symmetrical, the two-dimensional model could appropriately simulate the system hydrodynamics as well as a three-dimensional model, as in this study. However, a non-symmetrical system still needed a three-dimensional model that required a longer simulation time [36-39]. In addition, the effect of the reactor stage parameters on each MTO product yield was investigated. The studied reactor stage parameters were the number of reactor stages (A), the thickness of the reactor stage (B), and the wall temperature of the reactor stage (C). It was hypothesized that these reactor stage parameters affect the gas turbulence, catalyst residence time, and solid back-mixing, which then influence the yield of each product of the MTO reaction. The reactor stage will make the system be more dense and turbulent. This leads to more gas-solid contacting, solid-solid contacting and solid-wall contacting. Then, the catalyst momentum is lost and the catalyst residence time is longer.

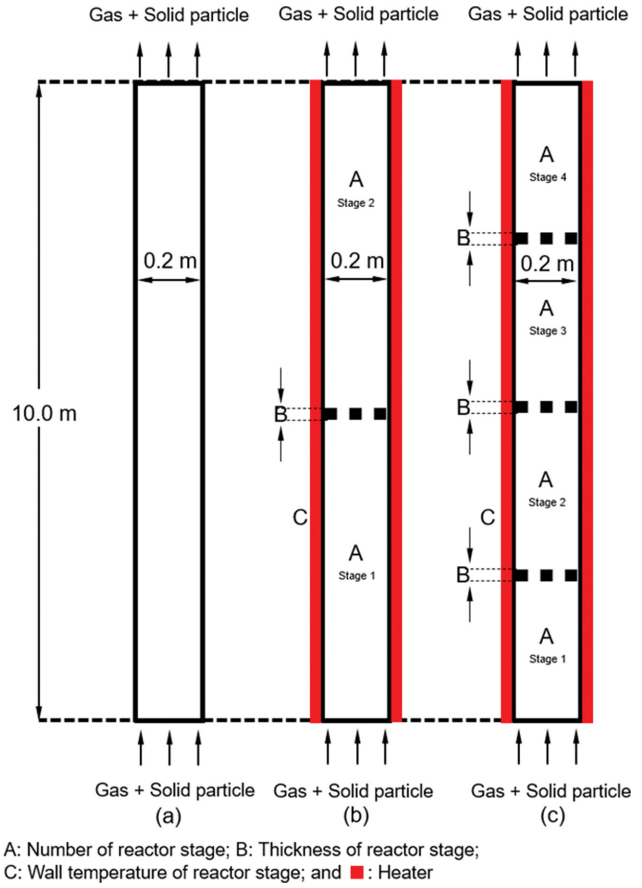

Fig. 1. Schematic drawing for (a) conventional MTO circulating fluidized bed riser and (b) stage MTO circulating fluidized bed reactor.

EXPERIMENTAL

1. CFD Hydrodynamics Simulation

In this study, the conventional MTO circulating fluidized bed riser from Soundararajan et al. [24] with a diameter of 0.2 m and a height of 10.0 m was selected as the base case study to validate the model as shown in Fig. 1(a). For the stage reactor, the stage MTO circulating fluidized bed riser was modified from the conventional MTO circulating fluidized bed riser by adding the thickness of reactor stage (B) in the system with forty percent opening surface area and equal spaces within and between the number of reactor stages (A). In addition, the wall temperature of reactor stage (C) was adjusted by the heater that was attached to the reactor wall of the circulating fluidized bed riser, as shown in Fig. 1(b).

For both MTO reactors, the gas and solid particles were fed at the bottom of the circulating fluidized bed riser with a constant velocity, while the gas and solid particles were vented at the top of the circulating fluidized bed riser.

In terms of the CFD hydrodynamics model, the employed conservation and constitutive equations from the kinetic theory of granular flow and the operating parameters /simulation setting are listed in Tables 1 and 2, respectively. Here, the commercial software ANSYS Fluent 18.0 was employed to solve the selected conservation and constitutive equations. The interphase exchange coefficient model was solved using an energy minimization multiscale (EMMS) model. This equation set was successfully used to simulate the hydrodynamics of the fluidized bed reactor [40], circulating fluidized bed reactor [1,27], and stage circulating fluidized bed reactor [28,40,41].

According to Phupanit et al. [41], a grid independence test of the same base case study was conducted using the grid number of 3,000, 6,000, 12,000, and 18,000 computational cells. In their results, the simulation results with 12,000 and 18,000 computational cells were not significantly different. Therefore, this study employed the case with 12,000 computational cells for both the conventional circulating fluidized bed riser and the stage circulating fluidized bed riser. For the time independence test, the result was that the simulation could reach its pseudo-steady state after 20 s. Thus, the simulated time was set as 40 s for all simulation cases with a time step size of 0.001 s. The simulation results from 20 to 40 s were then averaged and selected as a system representative. Regarding numerical accuracy, the simulation convergence criteria were set as 0.001

Table 1. The employed conservation and constitutive equations

Mass conservation equation of gas phase	$\frac{\partial(\varepsilon_g\rho_g)}{\partial t}+\nabla\cdot(\varepsilon_g\rho_g v_g)=0$
Mass conservation equation of solid particle phase	$\frac{\partial(\varepsilon_s\rho_s)}{\partial t}+\nabla\cdot(\varepsilon_s\rho_s v_s)=0$
Momentum conservation equation of gas phase	$\frac{\partial(\varepsilon_g\rho_g v_g)}{\partial t}+\nabla\cdot(\varepsilon_g\rho_g v_g v_g)=\nabla\cdot\tau_g-\varepsilon_g\nabla P_g+\varepsilon_g\rho_g g+\beta(v_g-v_s)$
Momentum conservation equation of solid particle phase	$\frac{\partial(\varepsilon_s\rho_s v_s)}{\partial t}+\nabla\cdot(\varepsilon_s\rho_s v_s v_s)=\nabla\cdot\tau_s-\varepsilon_s\nabla P_s+\varepsilon_s\rho_s g+\beta(v_g-v_s)$
Energy conservation equation of gas phase	$\frac{\partial}{\partial t}(\varepsilon_g\rho_g h_g)+\nabla\cdot(\varepsilon_g\rho_g h_g v_g)=-\varepsilon_g\frac{\partial P}{\partial t}+\tau_g:\nabla v_g$
Energy conservation equation of solid particle phase	$\frac{\partial}{\partial t}(\varepsilon_s\rho_s h_s)+\nabla\cdot(\varepsilon_s\rho_s h_s v_s)=-\varepsilon_s\frac{\partial P_s}{\partial t}+\tau_s:\nabla v_s$
Species conservation equation of gas phase	$\frac{\partial}{\partial t}(\rho_g\varepsilon_g Y_{g,i})+\nabla\cdot(\rho_g\varepsilon_g Y_{g,i}v_g)=-\nabla\cdot\varepsilon_g J_{g,i}+R_i$
Species conservation equation of solid particle phase	$\frac{\partial}{\partial t}(\rho_s\varepsilon_s Y_{s,i})+\nabla\cdot(\rho_s\varepsilon_s Y_{s,i}v_s)=-\nabla\cdot\varepsilon_s J_{s,i}+R_i$
Diffusive flux	$J_i=-\rho D_{i,m}\nabla Y_i$
Fluctuating kinetic energy conservation equation	$\frac{3}{2}\left[\frac{\partial}{\partial t}(\varepsilon_s\rho_s\theta_s)+\nabla\cdot(\varepsilon_s\rho_s v_s\theta_s)\right]=(-\nabla P_s I+\tau_s):\nabla v_s+\nabla\cdot(K_s\nabla\theta)-\gamma_s$
Stress tensor of gas phase	$\tau_g=\varepsilon_g\mu_g\left[\frac{1}{2}[\nabla\cdot v_g+(\nabla\cdot v_g)^T]-\frac{2}{3}(\nabla\cdot v_g)I\right]$
Stress tensor of solid particle phase	$\tau_s=\varepsilon_s\mu_s[\nabla\cdot v_s+(\nabla\cdot v_s)^T]-\varepsilon_s\left(\xi_s-\frac{3}{2}\mu_s\right)\nabla\cdot v_s$
Solid particle pressure	$P_s=2\rho_s(1+e)\varepsilon_s^2 g_0\theta_s+\varepsilon_s\rho_s\theta_s$
Solid particle radial distribution function	$g_0=\left[1-\left(\frac{\varepsilon_s}{\varepsilon_{s,max}}\right)^{1/3}\right]^{-1}$
Shear viscosity of solid particle phase	$\mu_s=\frac{4}{5}\varepsilon_s\rho_s d_p g_0(1+e)\sqrt{\frac{\theta}{\pi}}+\frac{10\rho_s d_p\sqrt{\pi\theta}}{96(1+e)g_0\varepsilon_s}\left[1+\frac{4}{5}\varepsilon_s g_0(1+e)\right]^2$
Solid particle bulk viscosity	$\xi_s=\frac{4}{3}\varepsilon_s\rho_s d_p g_0(1+e)\left(\frac{\theta_s}{\pi}\right)^{1/2}$
Solid particle diffusion coefficient of energy fluctuation	$\kappa_s=\frac{150\rho_s d_p\sqrt{\theta_s\pi}}{384(1+e)g_0}\left[1+\frac{6}{5}\varepsilon_s g_0(1+e)\right]^2+2\varepsilon_s^2\rho_s d_p g_0(1+e)\left(\frac{\theta_s}{\pi}\right)^{1/2}$
Solid particle collisional dissipation of energy fluctuation	$\gamma_s=3\varepsilon_s^2\rho_s g_0\theta_s(1-e)\left[\frac{4}{d_p}\left(\frac{\theta_s}{\pi}\right)^{1/2}\right]$
Gas-solid particle interphase exchange coefficient	$\beta_{gs}=150\frac{(1-\varepsilon_g)^2\mu_g}{\varepsilon_g d_p^2}+1.75\frac{(1-\varepsilon_g)\rho_g\lvert v_g-v_s\rvert}{d_p}$ When $\varepsilon_g<0.74$
	$\beta_{gs}=\frac{3(1-\varepsilon_g)\varepsilon_g}{4\ d_p}\rho_g\lvert v_g-v_s\rvert C_{D0}\omega(\varepsilon_g)$ When $\varepsilon_g\geq0.74$
	$\omega(\varepsilon_g)=-0.5760+\frac{0.0214}{4(\varepsilon_g-0.7463)^2+0.0044}$ When $0.74\leq\varepsilon_g<0.82$
	$\omega(\varepsilon_g)=-0.0101+\frac{0.0038}{4(\varepsilon_g-0.7789)^2+0.0040}$ When $0.82\leq\varepsilon_g<0.97$
	$\omega(\varepsilon_g)=-31.8295+32.8295\varepsilon_g$ When $\varepsilon\geq0.97$
	$C_{D0}=\frac{24}{Re}(1+0.15Re^{0.687})$ When $Re<1{,}000$
	$C_{D0}=0.44$ When $Re\geq1{,}000$
	$Re=\frac{d_p\rho_g\varepsilon_g\lvert v_g-v_s\rvert}{\mu_g}$

Table 2. The operating parameters of base case study and simulation settings

Operating parameter	Inlet solid particle mass flux	100 kg/m^{2}s
	Inlet gas superficial velocity	3.0 m/s
	Inlet reactor temperature	723 K
	Outlet reactor pressure	1.0×10^5 Pa
Gas (methanol)	Viscosity	1.8×10^{-5} kg/m s
	Density	1.184 kg/m^3
Solid particle - Catalyst (SAPO-34)	Diameter	80 μm
	Density	1,500 kg/m^3
Solid particle - Coke	Diameter	80 μm
	Density	2,000 kg/m^3
Simulation setting	Transient formulation	First-order implicit
	Pressure-velocity coupling	Phase coupled SIMPLE
	Momentum discretization	First-order upwind
	Volume fraction discretization	First-order upwind

Table 3. MTO reaction, reaction rate constant and catalyst deactivation factor

No.	Chemical reactions	Reaction rate constant (mol/($g_{catalyst}$ Pa s))	Catalyst deactivation factors (-)
1	$2CH_3OH\rightarrow C_2H_4+2H_2O$	$k_1=4.35\times10^{-3}\exp\left(\frac{-38{,}400}{RT}\right)$	$Ø_1=-3\times10^{-7}T^2+0.0006T-0.2365$
2	$3CH_3OH\rightarrow C_3H_6+3H_2O$	$k_2=5.56\times10^{-4}\exp\left(\frac{-27{,}000}{RT}\right)$	$Ø_2=-6\times10^{-7}T^2+0.0011T-0.4143$
3	$4CH_3OH\rightarrow C_4H_8+4H_2O$	$k_3=2.08\times10^{-4}\exp\left(\frac{-26{,}900}{RT}\right)$	$Ø_3=-9\times10^{-7}T^2+0.0014T-0.5148$
4	$5CH_3OH\rightarrow C_5H_{10}+5H_2O$	$k_4=6.94\times10^{-3}\exp\left(\frac{-49{,}800}{RT}\right)$	$Ø_4=-8\times10^{-7}T^2+0.0013T-0.4453$
5	$6CH_3OH\rightarrow C_6H_{12}+6H_2O$	$k_5=9.03\times10^{-3}\exp\left(\frac{-32{,}400}{RT}\right)$	$Ø_5=5\times10^{-6}T^2-0.0073T+2.9317$
6	$2CH_3OH\rightarrow C_{(S)}+CO_2+4H_2$	$k_6=3.53\times10^{-22}\exp\left(\frac{-6{,}707}{RT}\right)$	$Ø_6=-1\times10^{-6}T^2+0.0018T-0.7954$

in this study.

2. MTO Reaction Simulation

To apply the MTO reaction with conventional and stage circulating fluidized bed reactors, the employed MTO reaction models are shown in Eqs. (1) and (2), respectively. In this case, the components in the gas phase were methanol, ethene, propene, butene, pentene, hexene, carbon dioxide, hydrogen, nitrogen, and steam, while the components in the solid particle phase were carbon (coke) and SAPO-34 catalyst. Generally, the coke occurred on the catalyst particle. The occurrence of the coke on the catalysts affected catalyst deactivation. Therefore, the catalyst (SAPO-34) and coke were set in the same solid particle with a shared fraction. Two kinds of species were combined in the secondary phase (solid particle phase) with mixture material type. The overall reaction rate equations, obtained from Chang et al. [34], were modified by tuning the reaction rate constants to fit with the literature results [24,34,47].

$$R_i=k_i\,(1-ØC)\cdot Y_{oxygenate}\cdot P_A\cdot\rho_s\cdot\alpha_s \text{ where i=1-5} \quad (1)$$

$$R_6=k_6(1-ØC)\cdot X_{oxygenate}\cdot C_{A0}\cdot P_A\cdot\rho_s\cdot\alpha_s \quad (2)$$

where R_i is the rate of the arbitrary chemical reaction i, k_i is the rate constant of the arbitrary reaction i, C is the initial coke content of the catalyst, C_{A0} is the initial concentration of methanol, P_A is the initial partial pressure of methanol gas, Ø is the catalyst deactivation factors, ρ_s is the density of the catalyst, α_s is the volume ratio of the catalyst, $Y_{oxygenate}$ is the mole ratio of the oxygen compound, and $X_{oxygenate}$ is the percent conversion of the oxygen compound. The tuned reaction rate constants and the catalyst deactivation factors are shown in Table 3.

To calculate the reaction rates of the MTO reaction (Eqs. (1) and (2)), a user-defined function (UDF), written in C++ language, was developed. In this study, the rate of reverse reactions was not considered, as the equilibrium constant was very high. The high equilibrium constant could be calculated by the Gibbs free energy of each component based on the data given in [42].

3. Experimental Design for Reactor Stage Parameter Study

The 2^k factorial experimental design is widely used as a screening process for identifying the significant effects to the observed responses [43]. Moreover, it is successfully used to interpret the para-

Table 4. 2^k factorial experimental design for MTO reaction simulation

Case	Number of reactor stages (-) (A)	Thickness of reactor stage (mm) (B)	Wall temperature of reactor stage (K) (C)
No stage	-	-	-
1	2	0.5	673
2	4	0.5	673
3	2	10.0	673
4	4	10.0	673
5	2	0.5	773
6	4	0.5	773
7	2	10.0	773
8	4	10.0	773

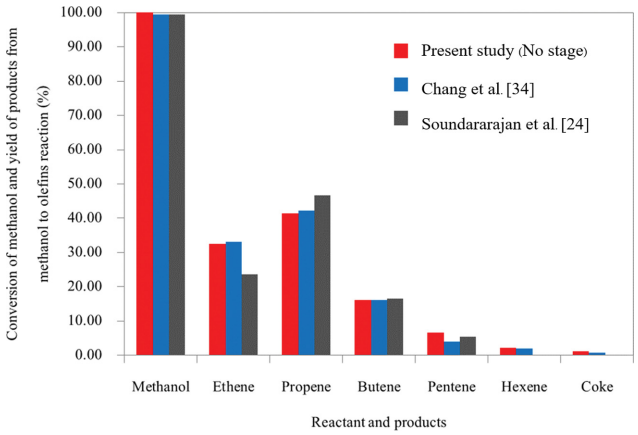

Fig. 2. Comparison of the predicted MTO reaction with literature data.

metric effects of a complicated system, such as the gas-solid fluidized bed system [44-46]. Thus, this study used this experimental design approach to analyze the main and interaction effects of the considered parameters where 2 is the level of considered parameters and k is the number of considered parameters. In this study, three reactor stage parameters were investigated using a 2^3 factorial experimental design approach including the number of reactor stages (A), the thickness of the reactor stage (B), and the wall temperature of the reactor stage (C). As stated above, each reactor stage parameter was varied with two parameter levels (low level and high level) for screening purposes or parametric trend observation. The reactor stage parameter levels were selected from the literature information and the material specifications [24,34]. In addition, the chemical reaction mostly occurred in lower part of reactor so, adding excess of the reactor stage insignificantly affected the product yield [31]. The 2^k factorial experimental design condition is summarized in Table 4. For the response parameter, the yield of the olefin product was considered to find the optimum parameter condition for obtaining each specific olefin product, including ethene, propene, light olefins (ethene and propene). The % selectivity (%Selectivity of A) and % yield of each olefin product (%Yield of A) can be calculated from Eq. (3) and Eq. (4).

$$\%\text{Selectivity of A} = \frac{\text{Product A}}{\text{Total products}} \times 100 \quad (3)$$

$$\%\text{Yield of A} = \frac{\%\text{Conversion} \times \%\text{Selectivity A}}{100} \quad (4)$$

Where %Conversion is the percentage of methanol conversion in the reaction and %Selectivity of A is the percentage of the concentration of desired Product A (mol/L) over the concentration of total products (mol/L).

RESULTS AND DISCUSSION

1. MTO Reaction Validation

For the MTO reaction model, this study compared the conversion of methanol and the yield of products with the literature results [24,34,47]. Both the results used the same reactor system, reactant and operating conditions. The overall reaction rates were modified by tuning the reaction rate constants to fit in the range of the literature results [24,34]. After the tuning of reaction rate constants, the suitable reaction rate constants for all the MTO reaction models were summarized as shown in Table 3. As stated in the experimental section, the yield of the olefin product from the conventional MTO circulating fluidized bed riser was compared. The obtained simulation results were consistent with those of the previous study, as illustrated in Fig. 2 and Table 5. The main products inside this reactor were propene, ethene, and butene. For the reactant conversion, the simulated conversion of methanol was 100%, while the conversion of methanol from Chang et al. [34] and Soundarara-

Table 5. Comparison of the predicted MTO reaction with literature data

Parameter	Present study (No stage) (-)	Chang et al., 2013 (-)	Soundararajan et al., 2001 (-)
Conversion of methanol (%)	100.00	99.42	99.40
Yield of ethene (%)	32.45	33.13	23.60
Yield of propene (%)	41.43	42.23	46.60
Yield of butene (%)	16.06	16.10	16.50
Yield of pentene (%)	6.60	4.06	5.40
Yield of hexene (%)	2.20	1.90	-
Yield of coke (%)	1.25	0.75	-

Table 6. Yields of MTO reaction

Case	Yield (%)						
	Ethene	Propene	Butene	Pentene	Hexene	Coke	Light olefins
No stage	32.45	41.43	16.06	6.60	2.20	1.25	73.88
1	27.75	47.00	18.04	3.76	2.21	1.24	74.75
2	27.61	46.98	18.03	3.81	2.20	1.37	74.59
3	27.32	47.34	18.18	3.70	2.20	1.26	74.66
4	29.31	45.50	17.45	4.33	2.23	1.17	74.81
5	27.45	47.22	18.13	3.75	2.20	1.25	74.67
6	27.36	47.02	18.05	3.77	2.19	1.61	74.38
7	28.34	46.41	17.81	3.99	2.22	1.24	74.74
8	28.88	45.82	17.58	4.22	2.22	1.29	74.69

Table 7. Analysis of variance for yield of ethene

Source of variation	SS	df	MS	F_0	p-Value
A	0.66	1	0.66	3,306.25	0.0111
B	1.69	1	1.69	8,464.00	0.0069
AB	0.95	1	0.95	4,761.00	0.0092
AC	0.24	1	0.24	1,225.00	0.0182
BC	0.16	1	0.16	812.25	0.0223
ABC	0.28	1	0.28	1,406.25	0.0170
Residual	2.000E-04	1	2.000E-04		
Total	4.00	7			

Note. SS: sum of squares; df: degree of freedom; MS: mean squares; F_0: F-statistic.

jan et al. [24] was about 99.40%. Thus, the computation error was acceptable, with a value of less than 1%.

Regarding hydrodynamic validation, the same MTO circulating fluidized bed riser was already validated by the hydrodynamics in Phupanit et al. [41]. Therefore, the developed CFD hydrodynamic model and MTO reaction model were well-validated. The developed model will be used later in this study.

2. Reactor Stage Parameter Study

Table 6 summarizes the yield of the MTO reaction according to the 2^k factorial experimental design in Table 4. As stated above, the main reaction product consideration of this study was the light olefins--ethene and propene. From Table 6, the yield of light olefins was higher for the stage circulating fluidized bed riser. This is because the gas and solid particle flow are more turbulent in the stage circulating fluidized bed risers than that of the conventional circulating fluidized bed riser, as shown and discussed in Phupanit et al. [41]. This behavior leads to higher interaction between catalyst solid particle and reactant gas. In addition, the modification of the reactor stage of the circulating fluidized bed riser decreased the yield of ethene but increased that of propene. This can be explained by the fact that the reaction rate of propene is higher than the reaction rate of ethene. From the thermodynamics analysis, the formation of propene was preferable when comparing the spontaneity of the reaction with the formation of ethene [42].

When compared with the conventional circulating fluidized bed riser, the yield of light olefins changed slightly when a stage circulating fluidized bed riser was used. However, the individual yields of each product were changed significantly. To obtain the maximum yield of ethene, propene, and light olefins, different reactor stage configurations were employed. For case 3, the two reactor stages with a 10 mm reactor stage thickness and 673 K wall temperature gave the highest yield of propene, with 47.34%. For case 4, the four reactor stages with 10 mm reactor stage thickness and 673 K wall temperature gave the highest yield of ethene and light olefins (ethene and propene), which were 29.31% and 74.81%, respectively. Even though the highest yield of light olefins insignificantly increased for the stage circulating fluidized bed reactor, but this design would promote the yield of propene and inferior yield of ethene.

For the reactor stage parametric evaluation, Table 7 sums up the analysis of variance for the yield of ethene. At the confidence interval of 95 percent, the parameters that have a p-value lower than 0.05 are identified as significant parameters. From the table, the main parameters that significantly affected the yield of ethene were the number of reactor stages (A) and the thickness of the reactor stage (B). The two-factor interaction parameters that significantly affected the yield of ethene were the interaction between the number of reactor stages and the thickness of the reactor stage (AB), the interaction between the number of reactor stages and the wall temperature of the reactor stage (AC) and the interaction between the thickness of the reactor stage and the wall temperature of the reactor stage (BC). In addition, the interaction between the number of reactor stages, the thickness of the reactor stage, and the wall temperature of the reactor stage (ABC) also had an effect on the yield of

Table 8. Analysis of variance of yield of propene

Source of variation	SS	df	MS	F_0	p-Value
A	2.196E-06	1	2.196E-06	10.74	0.0465
B	3.114E-06	1	3.114E-06	15.22	0.0299
AB	1.541E-06	1	1.541E-06	7.53	0.0710
ABC	6.304E-07	1	6.304E-07	3.08	0.1774
Residual	6.137E-07	3	2.046E-07		
Total	8.095E-06	7			

Note. SS: sum of squares; df: degree of freedom; MS: mean squares; F_0: F-statistic.

Table 9. Analysis of variance of yield of light olefins

Source of variation	SS	df	MS	F_0	p-value
A	4.512E-03	1	4.512E-03	1.35	0.3295
C	0.033	1	0.033	9.72	0.0526
AB	0.086	1	0.086	25.74	0.0148
ABC	0.014	1	0.014	4.07	0.1370
Residual	0.010	3	3.346E-03		
Total	0.15	7			

Note. SS: sum of squares; df: degree of freedom; MS: mean squares; F_0: F-statistic.

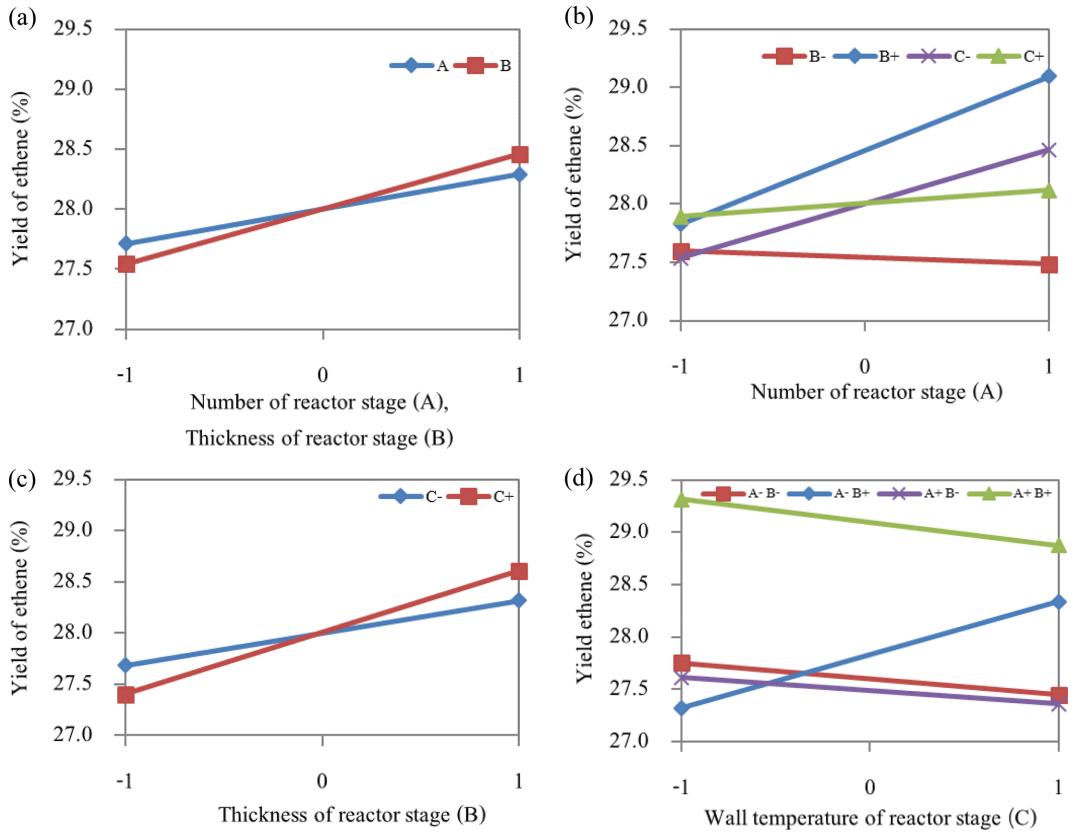

Fig. 3. The reactor stage parameter effect on the yield of ethene for (a) main parameter, (b) interaction of AB and AC, (c) interaction of BC and (d) interaction of ABC.

ethene. In Table 8, the analysis of variance for the yield of propene is summarized. The reactor stage parameters that had a significant effect on the yield of propene were only the number of reactor stages (A) and the thickness of the reactor stage (B). Table 9 shows the reactor stage parameters that significantly affected the yield of light olefins, which was only the interaction between the number

of reactor stages and the thickness of the reactor stage (AB).

Fig. 3(a) shows the main effect plot of the number of reactor stages (A) and the thickness of the reactor stage (B). The number of reactor stages (A) and the thickness of the reactor stage (B) had a positive effect on the yield of ethene. The increasing number of reactor stages (A) and the thickness of the reactor stage (B) could increase the yield of ethene. This is because the system is more turbulent according to the increasing gas velocity and the decreasing solid particle moving space. This is consistent with the obtained standard deviation of the solid volume fraction values in the horizontal direction [41]. These results also resemble the results of Zhu et al. [28] and Zhang et al. [40]. The solid particles were more turbulent and uniformly distributed in a stage circulating fluidized bed reactor as can be seen in Phupanit et al. [41]. Then, the yield of ethene was increased.

Fig. 3(b) shows the interaction effects between the number of reactor stages and the thickness of the reactor stage (AB) and between the number of reactor stages and the wall temperature of the reactor stage (AC). It was found that when the thickness of the reactor stage had a high value (B+) and the wall temperature of the reactor stage had a low (C−) or high (C+) value, the increase in the number of reactor stages (A) had a positive effect on the yield of ethene. The detailed definition of low and high values of each parameter is shown in Table 4. On the other hand, when the thickness of the reactor stage had a low value (B−), the increasing of the number of reactor stages (A) had a negative effect on the yield of ethene. Fig. 3(c) shows the interaction effect between the thickness of the reactor stage and the wall temperature of the reactor stage (BC). For both the high and low wall temperatures of the reactor stage, the increasing of the thickness of the reactor stage had a positive effect on the yield of ethene. As stated above, the increasing of the thickness of the reactor stage results in more solid particle flow restriction. The solid particles were more uniformly distributed throughout the system and had a longer residence time to react to achieve complete conversion of methanol as summarized in Phupanit et al. [41] and Ye et al. [48].

Fig. 3(d) shows the interaction plot between all three reactor stage parameters. For the yield of ethene, if the number of reactor stages had a high value (A+) and the thickness of the reactor stage had a low (B−) or high (B+) value, or the number of reactor stages had a low (A−) value and the thickness of the reactor stage had a low (B−) value, the increase of the wall temperature of the reactor stage (C+) had an adverse effect. A low yield of ethene was obtained when the temperature of the reactor wall increased.On the other hand, if the number of reactor stages had a low value (A−) and the thickness of the reactor stage had a high value (B+), the increase of the wall temperature of the reactor stage (C+) had a positive effect. This produced a higher yield of ethene. As stated above, the wall temperature of the reactor stage (C) had insignificant effect on the yield of ethene. However, due to the synergistic effect between reactor stage parameters, when the number of reactor stages had a low value (A−), the thickness of the reactor stage had a high value (B+) and the wall temperature of the reactor stage had a high value (C+), the solid particles had longer residence time and contact with the high temperature more than the other cases as can be seen in Phupanit et al. [41]. This would produce a higher yield of ethene.

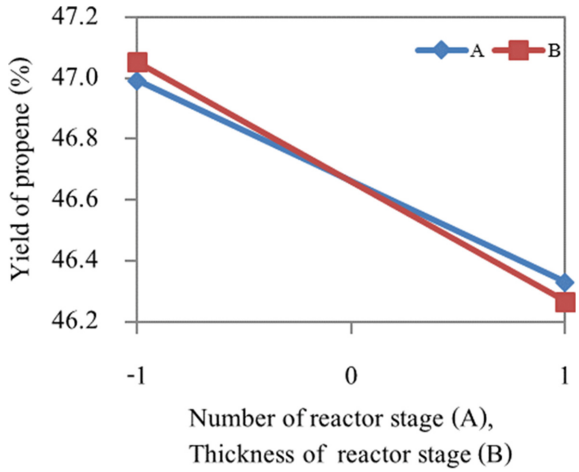

Fig. 4. The reactor stage parameter effect on the yield of propene for main parameter.

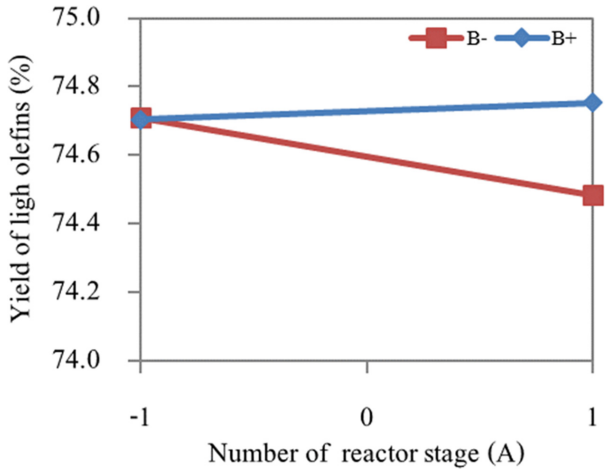

Fig. 5. The reactor stage parameter effect on the yield of light olefins for interaction of AB.

Fig. 4 shows the reactor stage parameters that affected the yield of propene. The number of reactor stages (A) and the thickness of the reactor stage (B) had a negative effect on the yield of propene. When the number of reactor stages (A) and the thickness of the reactor stage (B) were increased, lower yield of propene was obtained. The increasing number of reactor stages (A) and the thickness of the reactor stage (B) increased the residence time and caused more turbulence in the circulating fluidized bed riser [41]. In addition, from the reaction rate constants, ethene and butene were easier to form than propene. This decreased the yield of propene when residence time was increased. From the literature experiment, propene could be more easily cracked to form ethene [49]. However, the stage fluidized bed reactor had higher yield of propene than the conventional fluidized bed reactor.

Fig. 5 shows the interaction plot between the number of reactor stages and the thickness of the reactor stage (AB) that affected the yield of light olefins. If the thickness of the reactor stage had a high value (B+), the increase in the number of reactor stages (A) had a positive effect, but if the thickness of the reactor stage had a

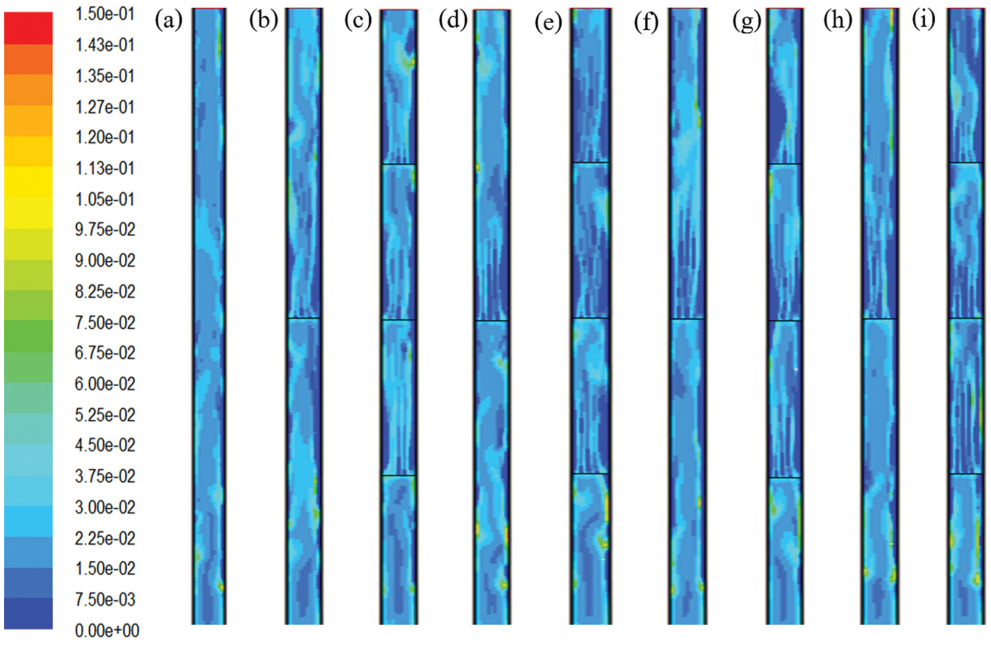

Fig. 6. Contours of solid volume fraction for (a) no stage riser, (b) case 1, (c) case 2, (d) case 3, (e) case 4, (f) case 5, (g) case 6, (h) case 7 and (i) case 8.

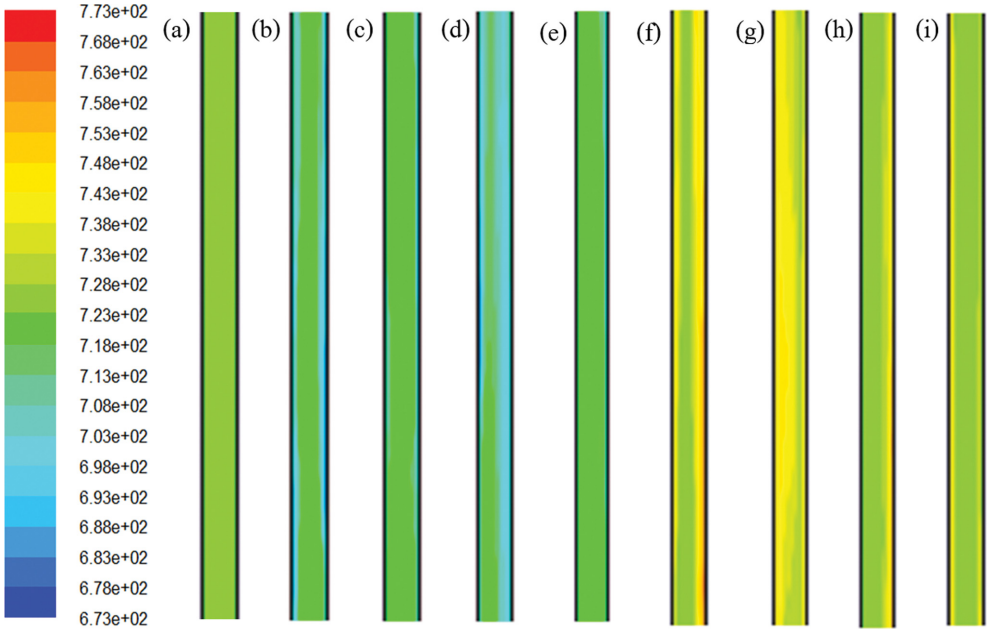

Fig. 7. Contours of gas temperature for (a) no stage riser, (b) case 1, (c) case 2, (d) case 3, (e) case4, (f) case 5, (g) case 6, (h) case 7 and (i) case 8.

low value (B−), the increase in the number of reactor stages (A) had a negative effect. This is because the increase of the reactor stages of the circulating fluidized bed riser with large thickness produced a lower solid particle residence time, while the increase of the reactor stages of the circulating fluidized bed riser with a smaller thickness produced a similar or higher solid particle residence time. The obtained solid particle residence time data were reported in Phupanit et al. [41].

To confirm the above explanation, the system hydrodynamics of both conventional and stage circulating fluidized bed risers was illustrated. Fig. 6 displays the contours of the solid volume fraction for conventional and stage circulating fluidized bed risers with various reactor stage cases in Table 4. It can be seen that when the conventional circulating fluidized bed riser was modified as a stage circulating fluidized bed riser, the system turbulence increased for all the reactor stage cases. The standard deviation of the horizontal solid volume fraction for conventional and stage circulating fluidized bed risers is shown in Phupanit et al [41]. The solid particles

were also denser in the stage circulating fluidized bed riser. This directly affected the contact time between the reactant gas and catalyst solid particle in the system. Fig. 7 depicts the distribution of the gas temperature in conventional and stage circulating fluidized bed risers. The temperature contours were consistent with the low and high wall temperatures of each reactor stage case in Table 4. The horizontal gas temperature was non-uniformly distributed, which was caused by the heat transfer inside the stage circulating fluidized bed riser [41]. At the location near the reactor stage, a high gas temperature was observed because the installation of the

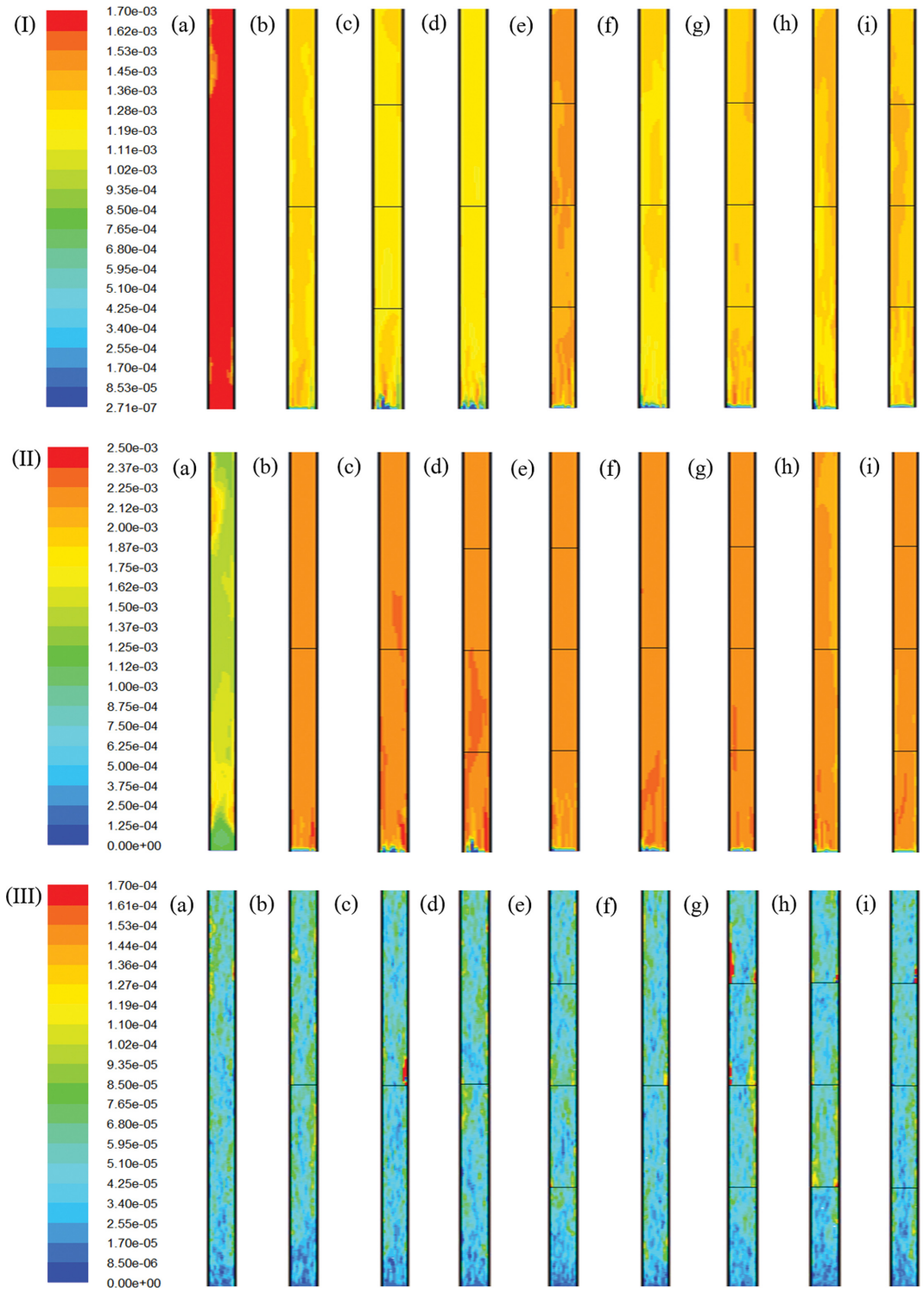

Fig. 8. Contours of concentration of (I) ethene, (II) propene and (III) coke for (a) no stage riser, (b) case 1, (c) case 2, (d) case 3, (e) case 4, (f) case 5, (g) case 6, (h) case 7 and (i) case 8.

reactor stage acted as a fin or extended surface, which promoted heat transfer at those areas. However, the increasing of the reactor stage wall temperature did not significantly affect the product yields similar to the literature results by Sedighi et al. [50]. Therefore, the different obtained results between the conventional circulating fluidized bed riser and the stage circulating fluidized bed riser were due to the increasing system turbulence. This confirms the above results that the effect of gas-solid mixing or stage configuration in the system was affected to product yields more than increased stage temperature.

To confirm the obtained results, in Table 6 it can be seen that the stage circulating fluidized bed riser decreased the yield of ethene but increased the yield of propene, compared to the conventional circulating fluidized bed riser, as shown in Figs. 8(I) and (II), respectively. From Fig. 8(I), ethene was uniformly distributed in both the vertical and horizontal directions of the circulating fluidized bed riser, and the highest concentration of ethene was found in case 4. From Fig. 8(II), propene was uniformly distributed in both the vertical and horizontal directions of the circulating fluidized bed riser, and the highest concentration of ethene was found in case 3. When the system had a longer contacting time or had more of a chemical reaction, the result was more accumulation of coke, as shown in Fig. 8(III). It showed that the coke was denser near the wall of the circulating fluidized bed riser but diluted in the center of the circulating fluidized bed riser. In addition, the lowest coke occurred in case 4, which had the highest ethene yield. This knowledge will help the engineer and technologist to better design and operate the conventional circulating fluidized bed reactor.

CONCLUSION

The hydrodynamics and MTO reaction model was successfully developed and coupled with the kinetic theory of granular flow model to simulate conventional and stage circulating fluidized bed risers. The reaction rates of the MTO reaction were optimized to match the literature experiment. Then, the effects of the number of reactor stages, the thickness of the reactor stage, and the wall temperature of the reactor stage were examined using a 2^3 statistical experimental design methodology. From the results, the increase in the number of reactor stages and the thickness of the reactor stage in the stage circulating fluidized bed riser decreased the ethene yield but increased the yield of propene as compared to the conventional fluidized bed riser. Moreover, the wall temperature of the reactor stage did not significantly affect the chemical reaction in the circulating fluidized bed riser. From the obtained solid volume fraction profile, the stage circulating fluidized bed riser could reduce the back-mixing and increase the system turbulence, which promotes the light olefins of the MTO reaction yield. However, by modifying the stage circulating fluidized bed riser, the yield of ethene decreased while the yields of propene and light olefins (ethene and propene) increased as compared to the conventional circulating fluidized bed riser. The highest yield of ethene and light olefins was found in case 4 (4 reactor stages, 10 mm reactor thickness, and 673 K reactor wall temperature), which yielded 29.31% and 74.81%, respectively. The highest yield of propene (47.34%) was found in case 3 (2 reactor stages, 10 mm reactor thickness, and 673 K reactor wall temperature). This work coupled the new design of the circulating fluidized bed riser with the MTO reaction. The advantage of the stage circulating fluidized bed reactor is illustrated. The results can also be used as a guideline to design and operate the conventional MTO or other chemical reaction circulating fluidized bed riser to obtain a higher yield/selectivity of products.

ACKNOWLEDGEMENT

The authors thank the Thailand Research Fund and National Research Council of Thailand for providing a Royal Golden Jubilee Ph.D. Program Grant, No. PHD/0011/2561. The authors also thank the National Research Council of Thailand and Chulalongkorn University for providing the Mid-Career Research Grant (NRCT5-RSA63001-24).

NOMENCLATURE

General Letters

A : number of reactor stage [-]
B : thickness of reactor stage [-]
C : wall temperature of reactor stage [-]
C : initial coke content of catalyst [%mol]
C_{A0} : initial concentration of methanol [mol/L]
C_{D0} : drag coefficient [-]
D : diffusivity [m^2/s]
d_p : solid particle diameter [m]
e : restitution coefficient [-]
g : gravity force [m/s^2]
g_0 : radial distribution function [-]
h : enthalpy [J/kg]
I : unit tensor [-]
J : diffusive flux [kg/m s]
k_i : rate constant of reaction [mol/($g_{catalyst}$ Pa s)]
P : pressure [Pa]
P_A : initial partial pressure of methanol gas [Pa]
R : gas constant [J/mol K]
Re : Reynolds number [-]
R_i : reaction rate [kmol/m^3 s]
t : time [s]
T : temperature [K]
v : velocity [m/s]
$X_{oxygenate}$: percent conversion of oxygen compound [%]
Y : mass fraction [-]
$Y_{oxygenate}$: mole ratio of oxygen compound [-]

Greek Letters

α_s : volume ratio of catalyst [-]
β : interphase exchange or drag coefficient model [kg/m^3 s]
ε : volume fraction [-]
$\varepsilon_{s,\max}$: solid volume fraction at maximum packing [-]
γ_s : collisional dissipation of solid particle fluctuating energy [J/m s^3]
κ_s : conductivity of solid particle fluctuating energy [kg/m s]
μ : viscosity [kg/m s]
θ : granular temperature [m^2/s^2]

ρ : density [kg/m^3]
ξ : bulk viscosity [kg/m s]
Ø : catalyst deactivation factors [-]
ω : drag correlation function [-]

Subscripts
g : gas phase
i : species
m : mixture
s : solid phase

REFERENCES

1. B. Chalermsinsuwan, T. Samruamphianskun and P. Piumsomboon, *Chem. Eng. Res. Des.*, **92**, 2479 (2014).
2. Y. Shi, X. Du, L. Yang, Y. Sun and Y. Yang, *Int. J. Hydrogen Energy*, **38**, 13974 (2013).
3. F. Ren, H. Li, D. Wang and J. Wang, *Prepr. Pap.-Am. Chem. Soc., Div. Fuel Chem.*, **48**, 921 (2003).
4. L. Zhu, N. Xie, P. Jiang, L. Li and H. Chen, *Chem. Eng. Res. Des.*, **114**, 247 (2016).
5. Z. Sun, W. Xiang and S. Chen, *Int. J. Hydrogen Energy*, **41**, 17323 (2016).
6. S. Ge, Z. Lou, Y. Yang, Z. Huang, J. Sun, J. Wang and Y. Yang, *AIChE J.*, **66**, 1 (2020).
7. P. Tian, Y. Wei, M. Ye and Z. Liu, *ACS Catal.*, **5**, 1922 (2015).
8. M. Stöcker, *Micropor. Mesopor. Mater.*, **29**, 3 (1999).
9. T. Álvaro-Muñoz, C. Márquez-Álvarez and E. Sastre, *Appl. Catal. A: Gen.*, **472**, 72 (2014).
10. F. Yaripour, Z. Shariatinia, S. Sahebdelfar and A. Irandoukht, *Micropor. Mesopor. Mater.*, **203**, 41 (2015).
11. F. L. Bleken, S. Chavan, U. Olsbye, M. Boltz, F. Ocampo and B. Louis, *Appl. Catal. A: Gen.*, **447-448**, 178 (2012).
12. S. Ivanova, C. Lebrun, E. Vanhaecke, C. Pham-Huu and B. Louis, *J. Catal.*, **265**, 1 (2009).
13. Q. Wang, L. Wang, H. Wang, Z. Li, H. Wu, G. Li, X. Zhang and S. Zhang, *Asia-Pacific J. Chem. Eng.*, **6**, 596 (2011).
14. Q. Yu, X. Meng, J. Liu, C. Li and Q. Cui, *Micropor. Mesopor. Mater.*, **181**, 192 (2013).
15. S. M. Sadrameli, *Fuel*, **140**, 102 (2015).
16. S. M. Sadrameli, *Fuel*, **173**, 285 (2016).
17. O. Awayssa, N. Al-Yassir, A. Aitani and S. Al-Khattaf, *Appl. Catal. A: Gen.*, **477**, 172 (2014).
18. J. Freiding and B. Kraushaar-Czarnetzki, *Appl. Catal. A: Gen.*, **391**, 254 (2011).
19. A. Izadbakhsh and F. Khorasheh, *Chem. Eng. Sci.*, **66**, 6199 (2011).
20. X. Huang, H. Li, H. Li and W.-D. Xiao, *Fuel Process. Technol.*, **150**, 104 (2016).
21. Y.-Q. Zhuang, X.-M. Chen, Z.-H. Luo and J. Xiao, *Comput. Chem. Eng.*, **60**, 1 (2014).
22. L. Bona, L. Hao, L. Hua, W. Wei, Y. Mao, L. Zhongmin and L. Jinghai, *Chem. Eng. Sci.*, **143**, 341 (2016).
23. H. Schoenfelder, J. Hinderer, J. Werther and F. J. Heil, *Chem. Eng. Sci.*, **49**, 5377 (1994).
24. S. Soundararajan, A. K. Dalai and F. Berruti, *Fuel*, **80**, 1187 (2001).
25. R. Gupta, V. Kumar and V. K. Srivastava, *Rev. Chem. Eng.*, **21**(2), 95 (2005).
26. R. Aramesh, V. Akbari, A. Shamiri, M. A. Hussain and N. Aghamohammadi, *Measurement*, **83**, 106 (2016).
27. B. Chalermsinsuwan, P. Kuchonthara and P. Piumsomboon, *Chem. Eng. Process.: Process Intensification*, **49**, 1144 (2010).
28. Y.-P. Zhu, F.-Z. Xiao and Z.-H. Luo, *Asia-Pacific J. Chem. Eng.*, **9**, 280 (2014).
29. S. Yang, L. Peng, W. Liu, H. Zhao, X. Lv, H. Li and Q. Zhu, *Powder Technol.*, **296**, 37 (2016).
30. Z. Yongmin, J. R. Grace, B. Xiaotao, L. Chunxi and S. Mingxian, *Chem. Eng. Sci.*, **64**, 3270 (2009).
31. T. Samruamphianskun, P. Piumsomboon and B. Chalermsinsuwan, *Chem. Eng. J.*, **210**, 237 (2012).
32. C.-W. Jiang, Z.-W. Zheng, Y.-P. Zhu and Z.-H. Luo, *Chem. Eng. Res. Des.*, **90**, 915 (2012).
33. G. Wu, Y. He and W. Chen, *Chem. Eng. J.*, **351**, 1104 (2018).
34. J. Chang, K. Zhang, H. Chen, Y. Yang and L. Zhang, *Chem. Eng. Res. Des.*, **91**, 2355 (2013).
35. Z. Jingyuan, L. Bona, C. Feiguo, L. Hua, Y. Mao and W. Wei, *Chem. Eng. Sci.*, **189**, 212 (2018).
36. B. Chalermsinsuwan and P. Piumsomboon, *Chem. Eng. Sci.*, **66**, 5602 (2011).
37. S. Cloete, S. Amini and S. T. Johansen, *Powder Technol.*, **205**, 103 (2011).
38. S. Cloete, S. T. Johansen and S. Amini, *Powder Technol.*, **239**, 21 (2013).
39. X. Lv, H. Li and Q. Zhu, *Chem. Eng. J.*, **236**, 149 (2014).
40. Y. Zhang, Q. Ma, X. Xu, Y. Xiao and F. Lei, *Chem. Eng. Process.: Process Intensification*, **98**, 71 (2015).
41. J. Phupanit, C. Soanuch, K. Korkerd, P. Piumsomboon and B. Chalermsinsuwan, *Asia-Pacific J. Chem. Eng.*, **14**, 1 (2018).
42. S. Aghamohammadi, M. Haghighi and M. Charghand, *Mater. Res. Bull.*, **50**, 462 (2014).
43. D. C. Montgomery, *Design and analysis of experiments*, Wiley and Sons, New York (2001).
44. S. Karimipour, R. Gerspacher, R. Gupta and R. J. Spiteri, *Fuel*, **103**, 308 (2013).
45. J.-H. Kim and J.-H. Rho, *Proc. IMechE, Part E: Process. Mech. Eng.*, **231**, 914 (2016).
46. T. Yurata, P. Piumsomboon and B. Chalermsinsuwan, *Chem. Eng. Res. Des.*, **153**, 401 (2020).
47. A. N. R. Bos and P. J. J. Tromp, *Ind. Eng. Chem. Res.*, **34**, 3808 (1995).
48. M. Ye, H. Li, Y. Zhao, T. Zhang and Z. Liu, *Adv. Chem. Eng.*, **47**, 279 (2015).
49. R. B. Rostami, M. Ghavipour, Z. Di, Y. Wang and R. M. Behbahani, *RSC Adv.*, **5**, 81965 (2015).
50. M. Sedighi, H. Bahrami and J. Towfighi, *J. Ind. Eng. Chem.*, **20**, 3108 (2014).